Materials Today Advances 12 (2021) 100177

Contents lists available at ScienceDirect

Materials Today Advances

journal homepage: www.journals.elsevier.com/materials-today-advances/

Metallic fusion of nanocrystal thin films for flexible and high-performance electromagnetic interference shielding materials

S. Park [a], J. Bang [b], B.-S. Kim [a], S.J. Oh [b, **], J.-H. Choi [a, *]

[a] Resources Utilization Research Center, Korea Institute of Geoscience and Mineral Resources, Daejeon, 34132, Republic of Korea
[b] Department of Materials Science and Engineering, Korea University, 145, Anam-ro Seongbuk-gu, Seoul, 02841, Republic of Korea

ARTICLE INFO

Article history:
Received 20 July 2021
Received in revised form
23 September 2021
Accepted 28 September 2021
Available online 29 October 2021

Keywords:
Nanocrystal
Ligand exchange
Electromagnetic interference shielding
Fusion
Sintering
Flexible devices

ABSTRACT

Low-cost flexible electromagnetic interference (EMI) shielding materials are attracting considerable attention because of the rapid development of wearable smart electronics, such as wearable health monitoring systems, and flexible energy storage and harvesting systems. In the present study, we developed ultrathin, flexible, and high-performance EMI shielding materials using Ag nanocrystals (NCs) through low-cost, room-temperature wet chemical processes conducted at atmospheric pressure. Sequential ligand-exchange and reduction processes not only substantially reduced the distance between the Ag NCs but also induced intensive metallic fusion of the Ag NCs, resulting in large-scale three-dimensional interconnected conductive pathways. The fused Ag NC thin films exhibited high electrical conductivity (~24,000 S/cm for a film ~800 nm thick) and outstanding mechanical stability, offering stable EMI shielding performance over 1000 cycles of various mechanical deformations, including twisting, crumpling, and folding. In addition, compared with most previously reported solution-based materials, our Ag NC thin films demonstrated an excellent EMI shielding effectiveness value of ~60 dB in the X-band range 8.2–12.2 GHz at much thinner thickness (~1.3 μm). With the advantages of easy processing, good mechanical flexibility, and high-performance EMI shielding, the fused NC thin films developed in the present work represent innovative potential EMI shielding materials for next-generation wearable smart electronics.

1. Introduction

With the rapid development of wireless telecommunication technology and the associated electronic devices, undesired electromagnetic interference (EMI) and radiation have become a serious problem that might adversely affect both people and the operation of devices [1,2]. Hence, high-performance EMI shielding materials with high shielding effectiveness (SE) have recently attracted attention [3–5]. Moreover, the rapid increase in popularity of wearable smart electronics has led to a need for EMI shielding materials that can be applied uniformly over a large area with minimal thickness on flexible substrates at low cost and at low temperatures.

Most EMI shielding materials currently in use are based on electrical conductors [6] such as metal-based, carbon-based, and conductive polymer materials [1,4,7]. Among these materials, the metal-based materials have been the most extensively used EMI shielding materials in commercial applications because of their high electrical conductivity [8,9]. However, traditional metal shrouds or sheets are poorly suited to applications requiring extensive deformation because of their lack of mechanical flexibility, and are fabricated by energy-intensive methods (vacuum deposition or sputtering) [10,11]. Therefore, extensive research efforts have focused on developing new EMI shielding materials that can be applied to flexible and scalable substrates while also demonstrating excellent shielding performance.

Colloidal Ag nanocrystals (NCs), also referred to as “nano-inks", are emerging as promising candidates for EMI shielding materials because of their easy processing, and low cost, and outstanding electrical conductivity [12–16]. Ag NCs can be synthesized on a large scale using wet chemical methods that provide thermodynamically stable colloidal solutions and are easily converted into large-area, flexible thin films via simple solution processes such as

* Corresponding author.
** Corresponding author.
E-mail addresses: sjoh1982@korea.ac.kr (S.J. Oh), jhchoi@kigam.re.kr (J.-H. Choi).

https://doi.org/10.1016/j.mtadv.2021.100177

spray-coating, roll-to-roll-coating, inkjet printing, and spin-coating. However, as-synthesized Ag NCs are capped with bulky electrically insulating organic ligands, which makes efficient charge transfer between Ag NCs difficult. As a result, Ag NCs do not retain their electronic properties and functionalities when Ag NC thin films are assembled into electronic devices. Conventional sintering processes, including laser and microwave sintering [17,18], high-temperature annealing [19–21], and electrolyte sintering [22], have been widely used to remove these ligands and ensure high conductivity. However, these methods require high temperatures or other complex procedures. By contrast, the ligand-exchange process is a simple yet effective solution-based route to modulate the electronic and electromechanical features of Ag NC thin films, enabling the rational design of Ag NC thin films for target applications [12,23,24]. Normally, upon exchange and removal of the native ligands on Ag NCs, the electronic coupling and movement of charge carriers across Ag NCs can be enhanced by reducing the distance between the Ag NCs. Furthermore, this shortened interparticle distance induces metallic fusion or sintering of the Ag NCs at room temperature and atmospheric pressure, leading to the formation of large-scale interconnected conductive networks [15,16,25]. Nevertheless, the suitability of conductive Ag NC thin films as high-performance flexible EMI shielding materials has rarely been studied.

In the present study, we fabricated highly conductive and flexible Ag NC thin films that exhibit excellent EMI SE and can be produced at room temperature and atmospheric pressure. Sequential ligand-exchange and reduction processes lead to the formation of three-dimensional (3D) interconnected structures through metallic fusion and aggregation of the Ag NCs while also eliminating nonmetallic compounds that impede efficient charge transport in the resultant Ag NC films, as confirmed by characterizing the structural, morphological, and optical properties of the Ag NC thin films. We also investigated the variation in electrical and electromechanical properties with increasing film thickness. The mechanical stability of the films was also analyzed via repetitive endurance tests under various mechanical deformations. The resultant Ag NC thin films exhibited excellent conductivity, flexibility, and EMI shielding performance and are thus suitable for use as next-generation conductive films to protect flexible and wearable electronic equipment from EMI.

2. Experimental section

2.1. Materials

Silver nitrate ($AgNO_3$, 99.9+%) was purchased from Alfa Aesar. Toluene (≥99.5%), (3-aminopropyl)triethoxysilane (APTES, 99%), tetrabutylammonium bromide (TBAB, ≥98%), sodium borohydride ($NaBH_4$, 99%), octane (≥99%), oleic acid (90%), and oleylamine (70%) were purchased from Sigma-Aldrich. Methyl alcohol (MeOH, 99.8%), ethyl alcohol (EtOH, 99.9%), and acetone (99.5%) were purchased from Samchun Chemical. Isopropyl alcohol (IPA, ≥99.5%) was purchased from Daejung Chemical. Polyimide (PI) films with a thickness of 5 μm were used as flexible substrates.

2.2. Synthesis of Ag NCs

Ag NCs were prepared using a previously reported wet chemical method [26]. Silver nitrate (1.7 g), 5 mL oleylamine, and 45 mL oleic acid were added to a 100 mL three-neck, round-bottom flask, mixed by magnetic stirring, and heated to 70 °C. The resultant mixture was degassed for 1.5 h while being maintained at 70 °C to remove moisture and oxygen. The temperature was then increased to 180 °C at 1 °C/min while Ar gas was injected. After the mixture reached 180 °C, it was allowed to cool in the air until the temperature decreased to room temperature. The solution was then washed several times with toluene (45 mL) and ethanol (120 mL) by centrifugation at 5000 rpm for 5 min. The washed Ag NCs were dispersed in octane at a concentration of 200 mg/mL.

2.3. Fabrication of Ag NC thin films

PI substrates were washed with acetone, IPA, and deionized water for 5 min each using a bath sonicator. They were then subjected to UV–ozone treatment for 30 min to remove contaminants and introduce –OH groups that improve adhesion. Finally, a 5 vol% APTES solution was spin-coated at 3000 rpm for 30 s to cover the surface of the substrate with amino groups, which can bond with functional groups (–COOH) in oleic acid. After pre-treatment of the substrates, conductive Ag NC thin films were fabricated via a simple chemical treatment. First, an Ag NC solution (200 mg/mL) was spin-coated onto the substrates at 1000 rpm for 30 s (Ag NC coating step). The substrates were then immersed in a TBAB solution (30 mM in MeOH) for 4 min and spin-coated at 3000 rpm for 10 s (ligand exchange step). They were then rinsed with MeOH at 3000 rpm for 30 s five times (rinsing step). Finally, they were spin-coated with a 0.5 vol% $NaBH_4$ solution at 3000 rpm for 60 s after being immersed in the $NaBH_4$ solution for 1 min for reduction (reduction step). The sequential process of Ag NC coating, ligand exchange (TBAB solution), rinsing (MeOH), and reduction ($NaBH_4$ solution) were performed 1 to 10 times to achieve the desired thickness. An Ag NC thin film fabricated using n repetitions was designated $(AgNC)_n$.

2.4. Characterization

The structure and morphology of the synthesized Ag NCs and Ag NC thin films were characterized by transmission electron microscopy (TEM, Tecnai G2 F30, FEI), field-emission scanning electron microscopy (FE-SEM, Hitachi SU8230, Hitachi High-Technologies), and X-ray diffraction (XRD, D/MAX-2200, Rigaku). Compositional analysis was performed using energy dispersive spectroscopy (EDS, MLA 650 FEG, FEI). Optical properties were measured using Fourier transform infrared (FT-IR) spectroscopy (Cary 630, Agilent Technologies) and ultraviolet–visible (UV–vis) spectrophotometry (S-4100, SCINCO). Electrical properties were measured using a four-probe station (MST 4000A, MSTECH), temperature controller (MST-1000H, MSTECH), and vacuum probe station (M5VC, MSTECH). Finally, electromagnetic shielding performance of the samples was characterized using a vector network analyzer (Agilent E8364B, Agilent Technologies).

3. Results and discussion

The procedures followed to fabricated the Ag NC thin films are depicted in Fig. 1. The detailed fabrication procedures are described in the Experimental section. Briefly, Ag NCs dispersed in octane were spin-coated onto a flexible substrate. To improve the conductivity of the film, ligand exchange and reduction steps were carried out using TBAB and $NaBH_4$ solutions, respectively. The TBAB replaced the long oleic acid ligands packed on the Ag NC surface with short Br^- ligands, decreasing the distance between particles. The Ag NCs were subsequently fused into large-scale solid Ag networks, as described in previous studies [15]. The reduction process was conducted by dipping the Ag NC thin films with Br^- ligands into a 0.5% $NaBH_4$ solution; the $NaBH_4$ solution removed the Br^- ions and reduced the Ag^+ ions to Ag^0 atoms. In this step, nonmetallic AgBr compounds, possibly formed during the ligand-

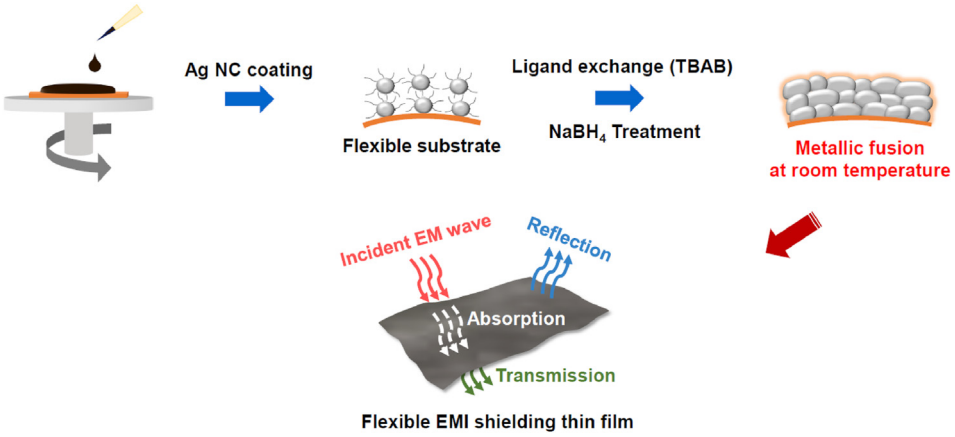

Fig. 1. Schematic illustration of the fabrication process of flexible and conductive Ag NC thin film for EMI shielding.

exchange process are removed from the Ag NC thin film [27]. The sequential processes of Ag NC coating, ligand exchange, and reduction were repeated multiple times (n). Through the above steps, highly conductive Ag NC thin films on flexible substrates were prepared at room temperature as high-performance EMI shielding materials.

The structural and chemical characteristics of the as-synthesized, ligand-exchanged, and reduced Ag NCs were analyzed (Fig. 2). Uniform spherical particles with an average diameter of 4.00 ± 0.26 nm were successfully synthesized (Fig. 2a). After ligand exchange, the Ag NCs were in close contact with each other and subsequently clustered into larger fused aggregates (Fig. 2b). After the reduction process, no substantial change was observed in the shape of the NCs; however, we confirmed that the size of the particles decreased because of the reduction of the nonmetallic compound AgBr (Fig. 2c). These ligand-exchange and reduction processes synergistically increase the possibility of contact between Ag NCs, which facilitates the interdiffusion of Ag atoms, leading to the fusion of the close-packed Ag NCs at room temperature.

XRD patterns were recorded to compare the structure of the Ag NC thin films before and after the ligand-exchange and reduction processes (Fig. 2d). The as-synthesized Ag NC thin films showed a broad peak at ~38.2° 2θ, which corresponds to the (111) plane of Ag. The broadening of the (111) peak is attributed to the small crystalline domains of the Ag NCs [28]. After the TBAB treatment for ligand exchange, the (111) peak became more intense and narrower, indicating grain growth in the Ag NC thin films via the fusion and aggregation of Ag NCs, consistent with the TEM observations. In addition, new peaks appeared at 31.1° (200), 44.3° (220), 64.5° (400), and 73.3° (420), which belong to AgBr (JCPDS 79–0148). After the $NaBH_4$ reduction step, new peaks attributable to crystalline Ag were observed at 38.0° (111), 44.3° (200), 64.3° (220), and 77.3° (311), whereas the peak associated with the AgBr phase completely disappeared. This result was further confirmed by elemental analysis, as shown in the SEM-EDS mapping and spectral images (Fig. S1). The removal of the AgBr phase via the reduction process might cause the larger polycrystalline NCs to break into a collection of smaller single-crystalline particles, leading to a decrease in the size of the NCs [15,29].

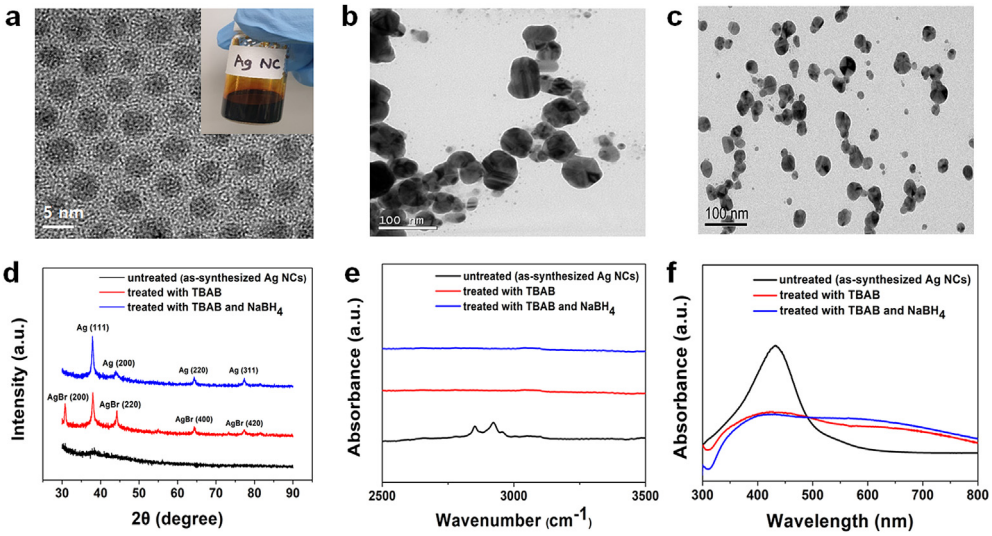

Fig. 2. (a) TEM images of synthesized Ag NCs, (b) after only TBAB treatment, and (c) both TBAB and $NaBH_4$ treatment. (d) XRD, (e) FT-IR, and (f) UV–Vis absorption spectra of Ag NC thin films untreated, treated with TBAB, and $NaBH_4$.

The FT-IR spectra in Fig. 2e show that, after the TBAB treatment, the absorption peaks near 2800–3000 cm^{-1} corresponding to a C–H stretching vibration disappeared. These peaks were also not present after the $NaBH_4$ treatment. These results indicate that oleic acid ligands surrounding the Ag NC surface were effectively replaced with Br^- by ligand exchange. Changes in the optical properties of the Ag NC thin films were analyzed by UV–vis spectrophotometry (Fig. 2f). The spectrum of the untreated film shows a broad and intense absorption peak at ~430 nm. This peak, which is attributed to the localized surface plasmonic resonance of the Ag NCs [30], disappeared after the TBAB treatment, indicating that the characteristics of the isolated NCs were not observed in the film as a result of the ligand exchange and/or the reduction treatment.

The thickness and morphology of the Ag NC thin films fabricated using different numbers of spin-coating cycles were examined by FE-SEM. Fig. 3a–c shows cross-sectional images of $(AgNC)_3$, $(AgNC)_6$, and $(AgNC)_8$; the thicknesses of these films were 503 nm, 809 nm, and 1.06 μm, respectively. The variation in overall thickness of all fabricated samples as a function of the number of repetitions (n) is presented in Fig. S2. The cross-sectional images clearly revealed that the Ag NCs had fused and aggregated to form a 3D interconnected structure, which also appeared in the surface SEM image of the Ag NC thin film (Fig. S3). Moreover, the thickness of the deposited film increased with the number of repetitions, reaching up to ~1.3 μm for $(AgNC)_{10}$, but the rate of increase was not constant. To investigate this behavior in detail, we measured the weight of the samples after each deposition cycle (Fig. 3d). Although the magnitude of the weight gain gradually decreased as the deposition was repeated because of solvent evaporation associated with the spin-coating method [31], we confirmed that the electrical and electromechanical properties improved with increasing repetition number, as described later in this section. In addition, as shown in Fig. S4, the densities of the Ag NC thin films with different n values were similar, with an average value for all films of 9.00 ± 0.15 g/cm^3.

We further studied the electrical properties of the Ag NC thin films as a function of the repetition number. Fig. 3e shows the sheet resistance and electrical conductivity of the Ag NC thin films deposited on PI sheets as a function of repetition number n. As increased from 2 to 10, the sheet resistance (R_s) decreased from 3.78 to 0.312 Ω/square. The R_s of $(AgNC)_1$ is not included here because it showed poor reproducibility. In general, the loss of ligand volume resulting from the ligand exchange process leads to the formation of cracks and pinholes in the films that impede efficient charge transport [32,33]. The R_s value decreased markedly with increasing the number of cycles up to 5–6, reaching 0.52 Ω/square, which is comparable to the R_s of vacuum-deposited Ag (0.45 Ω/square). The decrease in R_s may be due to repeated cycles filling in cracks in the underlying layer, thereby forming more stable and continuous conductive networks across the entire film. When the repetition number was further increased from 6 to 10, the R_s of the Ag NC thin films was insensitive to the film thickness. These results suggest that six cycles are sufficient to produce a film with efficient electrical properties. Indeed, as shown in the inset in Fig. 3e, the highest electrical conductivity (24,038 S/cm) was observed for $(AgNC)_6$, with the conductivity decreasing slightly as the repetition number increased from 6 to 8.

We also observed the temperature dependence of the resistance of the Ag NC thin film to understand the metallic electron transfer mechanism (Fig. 3f). The resistance of $(AgNC)_3$ fabricated on a glass substrate was measured every 20 K as the temperature was lowered from 300 to 100 K. The ratio of the resistance measured at temperature T to the resistance at 100 K (R_T/R_0) decreased linearly and slowly with decreasing temperature, indicating a positive temperature coefficient of resistance (TCR). This result explains the metallic behavior, where the increase in atomic vibrations with increasing temperature causes electrons to be more scattered, thereby increasing the resistance. The TCR value ($\alpha = 0.000635\ K^{-1}$) was calculated using the equation $\alpha = \{(\Delta R/R_0)\}/\Delta T$, where R and R_0 are the resistance values at 300 and 100 K, respectively.

To explore the adaptability of the fused Ag NC thin film for various epidermal and wearable applications, we examined its mechanical stability. Fig. 4a shows the variation in R/R_0 of the Ag NC thin films as a function of their bending radius (0.5, 0.8, 1.5, and 2.5 mm). Representative $(AgNC)_6$ prepared on PI sheets exhibited outstanding durability at bending radii as small as 0.5 mm. In

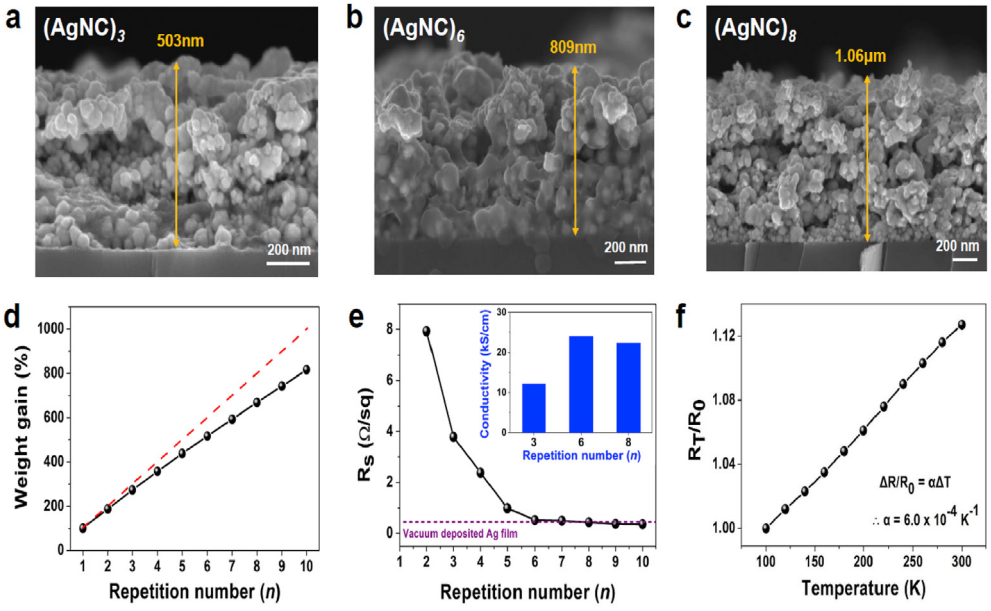

Fig. 3. (a–c) Cross-sectional SEM images of Ag NC thin films, (d) Weight gain rate, (e) Sheet resistance, and electrical conductivity of Ag NC thin films according to the repetition number of spin-coating cycles. (f) Resistance change of $(AgNC)_3$ as the temperature is decreased from 300 to 100 K.

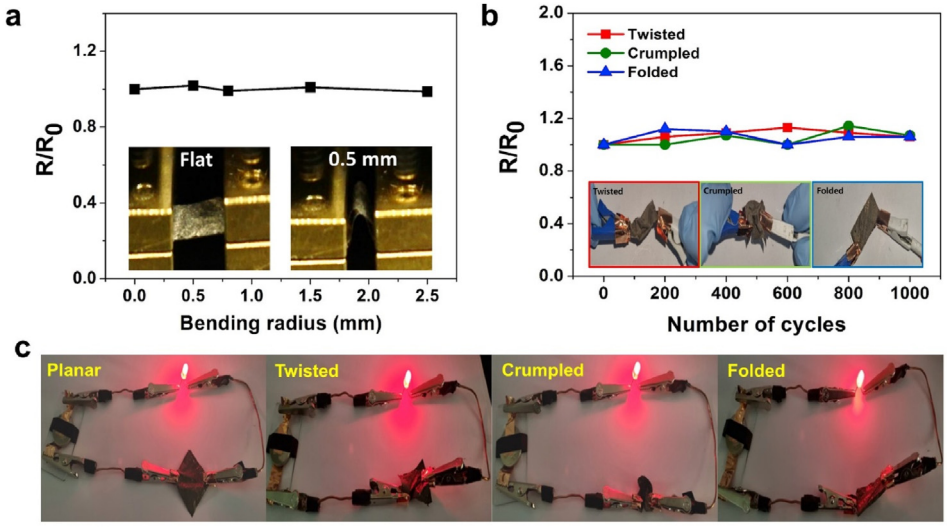

Fig. 4. (a) Resistance changes of $(AgNC)_6$ in response to bending radius (0.5, 0.8, 1.5, and 2.5 mm), and (b) repetitive cycles according to various strain forms (crumpled, twisted, and folded) of flexible $(AgNC)_6$. (c) Photographs of flexible $(AgNC)_6$. The red diodes were still lit under various deformations.

addition, to demonstrate the extreme flexibility of the films, repetitive mechanical deformation tests, including twisting, crumpling, and folding tests, were conducted (Fig. 4b). For these tests, Ag NC thin films were fabricated on highly flexible substrates (5 μm-thick PI sheets). Even after 1000 cycles of the three mechanical deformation modes, the films did not show a substantial change in resistance. Finally, we used these Ag NC thin films to fabricate mechanically flexible and stable electrical connections with a red light-emitting diode (Fig. 4c).

Next we considered the EMI shielding properties of the highly conductive and flexible Ag NC thin films. When EM radiation strikes a material, three different shielding mechanisms are possible: reflection, absorption, and multiple internal reflections (abbreviated as SE_R, SE_A, and SE_M, respectively) [34]. For conductive materials, the EMI shielding ability depends on the intrinsic electrical properties of the material (i.e., permeability, dielectric constant, and conductivity), as shown in the following equations [35,36]:

$$SE_T = SE_R + SE_A + SE_M \tag{1}$$

$$SE_R = 39.5 + 10log\frac{\sigma}{2f\pi\mu} \propto \sigma/\mu \tag{2}$$

$$SE_A = 8.7d\sqrt{f\pi\sigma\mu} \propto d\sigma\mu \tag{3}$$

$$SE_M = 20log(1 - e^{\frac{-2d}{\delta}}) \tag{4}$$

$$\delta = (f\pi\sigma\mu)^{-1/2} \tag{5}$$

Here, σ is the total conductivity, f is the frequency, μ is the relative permeability, d is the sample thickness, and δ is the skin depth. According to these equations, the σ and d of EMI shielding materials are important parameters for both the reflection and absorption of EM waves. However, because an increase in thickness typically leads to an increase in weight, it is important to achieve high-efficiency shielding performance with thin thickness. The multiple internal reflection component, SE_M, can be neglected when SE_T is greater than 15 dB [37]. The Ag NC thin films presented in the present work, which exhibit high conductivity, demonstrated good EMI shielding performance, with a small thickness of ~1 μm. The EMI SE can be expressed on the basis of the S-parameters (S_{11} and S_{21}) and can be calculated according to the following equations [38–40]:

$$SE_T = SE_R + SE_A = 10\log(\frac{1}{|S_{21}|^2}) \tag{6}$$

$$SE_R = 10\log(\frac{1}{1 - |S_{11}|^2}) \tag{7}$$

$$SE_A = 10log(\frac{1 - |S_{11}|^2}{|S_{21}|^2}) \tag{8}$$

Fig. 5a and S5 show the total EMI shielding effectiveness (SE_T) as a function of increasing the repetition number, n. When n was increased from 1 to 10, the average SE_T values ranged from 0.23 dB to 59 dB in the X-band frequency range (8.2–12.2 GHz). When n was greater than 3, the SE_T value was greater than 20 dB, which is the requirement for practical applications [41]. Notably, the SE_T value for $(AgNC)_6$ (~52 dB) was close to that of the vacuum deposited Ag film (~51 dB), as shown in Fig. S5. The values of the reflection (SE_R, Fig. 5b) and absorption (SE_A, Fig. 5c) components of SE of the Ag NCs thin films were also compared and analyzed to gain further insight into their shielding mechanism. Interestingly, the SE_A values steadily increased with increasing thickness, consistent with the trend observed for SE_T, whereas the SE_R value plateaued on going to films thicker than $(AgNC)_6$, indicating the dominant contribution of SE_A to the enhancement of SE_T. We further examined the change in EMI SE of $(AgNC)_6$ when the film was subjected to various strains (twisting, crumpling, and folding) (Fig. 5d). Even after 1000 cycles, the EMI shielding properties remained above 50 dB, which is comparable to the value of the undeformed $(AgNC)_6$, indicating that the mechanical deformation did not significantly affect the EMI SE (Fig. 4d). These results demonstrate that the Ag NC thin films developed in the present work show excellent EMI SE and good flexibility, and hence are suitable for use in epidermal and wearable devices that are subjected to strains resulting from various movements. A comparison of total EMI SE in the X-band between the Ag NC thin films and other reported materials is given in Fig. 5e and Table S1. This

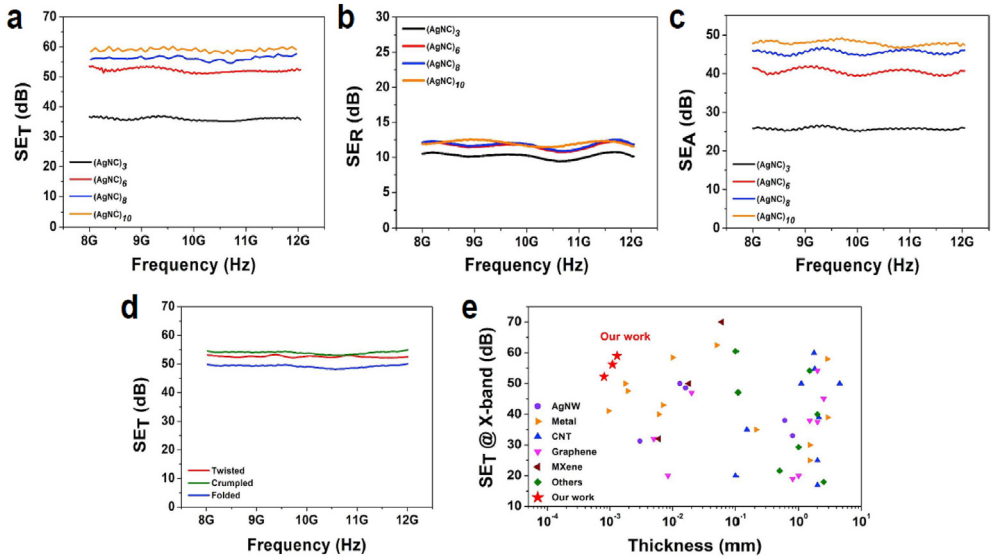

Fig. 5. (a) Total EMI SE (SE_T) (b) reflection SE (SE_R), and (c) absorption SE (SE_A) of Ag NC films versus frequency (from 8.2 to 12.2 GHz) with the different number of repetition. (d) EMI SE changes of $(AgNC)_6$ after diverse deformations. (e) Total EMI SE as a function of thickness for different shielding materials.

comparison shows that the Ag NC films reported here exhibit sufficiently good EMI SE values at much thinner thickness compared with most previously reported materials. The high EMI SE of the Ag NC films, which can be produced at room temperature using a simple and inexpensive solution process, shows their strong potential as EMI shielding materials for commercial applications in which thinness and flexibility are important.

4. Conclusion

In summary, we fabricated highly conductive Ag NC thin films with outstanding mechanical flexibility and efficient EMI shielding performance at room temperature using simple wet-chemical processes. The fused Ag NC thin films achieved using ligand-exchange and reduction processes were clearly interconnected through the metallic fusion and aggregation of Ag NCs. The resultant Ag NC thin films, which were fabricated on flexible substrates using the proposed approach, exhibited a maximum EMI SE of ~60 dB with a thickness of ~1.3 μm and excellent mechanical stability under various mechanical deformations. The flexible Ag NC thin films with excellent EMI-shielding performance reported here thus have strong potential for use in aerospace and wearable smart electronics applications.

Credit author contribution statement

Seoyeon Park: Investigation, Formalanalysis, Validation, Writing - original draft. **Junsung Bang& Byung-su Kim**: Methodology and Writing – Review & Editing. **Ji-Hyuk Choi** & **Soong Ju Oh**: Conceptualization, Investigation, Data analysis, Project administration, Review & Editing, Supervision.

Declaration of competing interest

The authors declare that they have no known competing financial interests or personal relationships that could have appeared to influence the work reported in this paper.

Acknowledgements

This work was supported by the Basic Research Project (Grant Number: 21-3212-1) of the Korea Institute of Geoscience and Mineral Resources funded by the Ministry of Science and ICT of Korea. This work was also funded by the National Research Foundation of Korea 2018R1C1B6002958(19-6818).

Appendix A. Supplementary data

Supplementary data to this article can be found online at https://doi.org/10.1016/j.mtadv.2021.100177.

References

[1] M. Hu, J. Gao, Y. Dong, K. Li, G. Shan, S. Yang, R.K. Li, Flexible transparent PES/silver nanowires/PET sandwich-structured film for high-efficiency electromagnetic interference shielding, Langmuir 28 (2012) 7101–7106, https://doi.org/10.1021/la300720y.
[2] A.P. Singh, M. Mishra, D.P. Hashim, T.N. Narayanan, M.G. Hahm, P. Kumar, J. Dwivedi, G. Kedawat, A. Gupta, B.P. Singh, A. Chandra, R. Vajtai, S.K. Dhawan, P.M. Ajayan, B.K. Gupta, Probing the engineered sandwich network of vertically aligned carbon nanotube–reduced graphene oxide composites for high performance electromagnetic interference shielding applications, Carbon 85 (2015) 79–88, https://doi.org/10.1016/j.carbon.2014.12.065.
[3] R.R. Mohan, S.J. Varma, M. Faisal, J. S, Polyaniline/graphene hybrid film as an effective broadband electromagnetic shield, RSC Adv. 5 (2015) 5917–5923, https://doi.org/10.1039/C4RA13704C.
[4] J. Liu, H.B. Zhang, R. Sun, Y. Liu, Z. Liu, A. Zhou, Z.Z. Yu, Hydrophobic, flexible, and lightweight MXene foams for high-performance electromagnetic-interference shielding, Adv. Mater. 29 (2017) 1702367, https://doi.org/10.1002/adma.201702367.
[5] Z. Chen, C. Xu, C. Ma, W. Ren, H.M. Cheng, Lightweight and flexible graphene foam composites for high-performance electromagnetic interference shielding, Adv. Mater. 25 (2013) 1296–1300, https://doi.org/10.1002/adma.201204196.
[6] M. Arjmand, A.A. Moud, Y. Li, U. Sundararaj, Outstanding electromagnetic interference shielding of silver nanowires: comparison with carbon nanotubes, RSC Adv. 5 (2015) 56590–56598, https://doi.org/10.1039/C5RA08118A.
[7] Y.J. Wan, X.Y. Wang, X.M. Li, S.Y. Liao, Z.Q. Lin, Y.G. Hu, T. Zhao, X.L. Zeng, C.H. Li, S.H. Yu, P.L. Zhu, R. Sun, C.P. Wong, Ultrathin densified carbon nanotube film with "Metal-like" conductivity, superior mechanical strength, and ultrahigh electromagnetic interference shielding effectiveness, ACS Nano 14 (2020) 14134–14145, https://doi.org/10.1021/acsnano.0c06971.
[8] F. Fang, Y.-Q. Li, H.-M. Xiao, N. Hu, S.-Y. Fu, Layer-structured silver nanowire/polyaniline composite film as a high performance X-band EMI shielding material, J. Mater. Chem. C 4 (2016) 4193–4203, https://doi.org/10.1039/C5TC04406E.

[9] Y. Chen, Y. Li, M. Yip, N. Tai, Electromagnetic interference shielding efficiency of polyaniline composites filled with graphene decorated with metallic nanoparticles, Compos. Sci. Technol. 80 (2013) 80–86, https://doi.org/10.1016/j.compscitech.2013.02.024.
[10] S. Lin, H. Wang, F. Wu, Q. Wang, X. Bai, D. Zu, J. Song, D. Wang, Z. Liu, Z. Li, N. Tao, K. Huang, M. Lei, B. Li, H. Wu, Room-temperature production of silver-nanofiber film for large-area, transparent and flexible surface electromagnetic interference shielding, npj Flex. Electron. 3 (2019) 1–8, https://doi.org/10.1038/s41528-019-0050-8.
[11] H. Ji, R. Zhao, N. Zhang, C. Jin, X. Lu, C. Wang, Lightweight and flexible electrospun polymer nanofiber/metal nanoparticle hybrid membrane for high-performance electromagnetic interference shielding, NPG Asia Mater. 10 (2018) 749–760, https://doi.org/10.1038/s41427-018-0070-1.
[12] D.V. Talapin, J.-S. Lee, M.V. Kovalenko, E.V. Shevchenko, Prospects of colloidal nanocrystals for electronic and optoelectronic applications, Chem. Rev. 110 (2010) 389–458, https://doi.org/10.1021/cr900137k.
[13] A.T. Fafarman, S.-H. Hong, S.J. Oh, H. Caglayan, X. Ye, B.T. Diroll, N. Engheta, C.B. Murray, C.R. Kagan, Air-stable, nanostructured electronic and plasmonic materials from solution-processable, silver nanocrystal building blocks, ACS Nano 8 (2014) 2746–2754, https://doi.org/10.1021/nn406461p.
[14] J.-H. Choi, H. Wang, S.J. Oh, T. Paik, P. Sung, J. Sung, X. Ye, T. Zhao, B.T. Diroll, C.B. Murray, Exploiting the colloidal nanocrystal library to construct electronic devices, Science 352 (2016) 205–208, https://doi.org/10.1126/science.aad0371.
[15] M.S. Kang, H. Joh, H. Kim, H.W. Yun, D. Kim, H.K. Woo, W.S. Lee, S.H. Hong, S.J. Oh, Synergetic effects of ligand exchange and reduction process enhancing both electrical and optical properties of Ag nanocrystals for multifunctional transparent electrodes, Nanoscale 10 (2018) 18415–18422, https://doi.org/10.1039/C8NR05212C.
[16] Y. Song, D. Kim, S. Kang, Y. Ko, J. Ko, J. Huh, Y. Ko, S.W. Lee, J. Cho, Room-temperature metallic fusion-induced layer-by-layer assembly for highly flexible electrode applications, Adv. Funct. Mater. 29 (2019) 1806584, https://doi.org/10.1002/adfm.201806584.
[17] J. Niittynen, R. Abbel, M. Mäntysalo, J. Perelaer, U.S. Schubert, D. Lupo, Alternative sintering methods compared to conventional thermal sintering for inkjet printed silver nanoparticle ink, Thin Solid Films 556 (2014) 452–459, https://doi.org/10.1016/j.tsf.2014.02.001.
[18] P. Laakso, S. Ruotsalainen, E. Halonen, M. Mäntysalo, A. Kemppainen, Sintering of printed nanoparticle structures using laser treatment, in: international Congress on Applications of Lasers & Electro-Optics, J. Laser Appl. (2009) 1360–1366, https://doi.org/10.2351/1.5061499.
[19] Y.-L. Tai, Z.-G. Yang, Fabrication of paper-based conductive patterns for flexible electronics by direct-writing, J. Mater. Chem. 21 (2011) 5938–5943, https://doi.org/10.1039/C0JM03065A.
[20] B.Y. Ahn, E.B. Duoss, M.J. Motala, X. Guo, S.I. Park, Y. Xiong, J. Yoon, R.G. Nuzzo, J.A. Rogers, J.A. Lewis, Omnidirectional printing of flexible, stretchable, and spanning silver microelectrodes, Science 323 (2009) 1590–1593, https://doi.org/10.1126/science.1168375.
[21] S. Ji, W. He, K. Wang, Y. Ran, C. Ye, Thermal response of transparent silver nanowire/PEDOT:PSS film heaters, Small 10 (2014) 4951–4960, https://doi.org/10.1002/smll.201401690.
[22] M. Layani, M. Grouchko, S. Shemesh, S. Magdassi, Conductive patterns on plastic substrates by sequential inkjet printing of silver nanoparticles and electrolyte sintering solutions, J. Mater. Chem. 22 (2012) 14349–14352, https://doi.org/10.1039/C2JM32789A.
[23] A.T. Fafarman, W.-k. Koh, B.T. Diroll, D.K. Kim, D.-K. Ko, S.J. Oh, X. Ye, V. Doan-Nguyen, M.R. Crump, D.C. Reifsnyder, Thiocyanate-capped nanocrystal colloids: vibrational reporter of surface chemistry and solution-based route to enhanced coupling in nanocrystal solids, J. Am. Chem. Soc. 133 (2011) 15753–15761, https://doi.org/10.1021/ja206303g.
[24] C.R. Kagan, Flexible colloidal nanocrystal electronics, Chem. Soc. Rev. 48 (2019) 1626–1641. https://di.org/10.1039/C8CS00629F.
[25] S.-W. Lee, H. Joh, M. Seong, W.S. Lee, J.-H. Choi, S.J. Oh, Transition states of nanocrystal thin films during ligand-exchange processes for potential applications in wearable sensors, ACS Appl. Mater. Interfaces 10 (2018) 25502–25510, https://doi.org/10.1021/acsami.8b06754.
[26] J. Park, S.G. Kwon, S.W. Jun, B.H. Kim, T. Hyeon, Large-scale synthesis of ultra-small-sized silver nanoparticles, ChemPhysChem 13 (2012) 2540–2543, https://doi.org/10.1002/cphc.201101035.
[27] G.S. Perera, S.M. Ansar, S. Hu, M. Chen, S. Zou, C.U. Pittman, D. Zhang, Ligand desorption and desulfurization on silver nanoparticles using sodium borohydride in water, J. Phys. Chem. C 118 (2014) 10509–10518, https://doi.org/10.1021/jp5025526.
[28] M. Zienkiewicz-Strzałka, S. Pasieczna-Patkowska, M. Kozak, S. Pikus, Silver nanoparticles incorporated onto ordered mesoporous silica from Tollen's reagent, Appl. Surf. Sci. 266 (2013) 337–343, https://doi.org/10.1016/j.apsusc.2012.12.021.
[29] Z. Zhang, Y. Wu, Investigation of the NaBH4-induced aggregation of Au nanoparticles, Langmuir 26 (2010) 9214–9223, https://doi.org/10.1021/la904410f.
[30] M. Rycenga, C.M. Cobley, J. Zeng, W. Li, C.H. Moran, Q. Zhang, D. Qin, Y. Xia, Controlling the synthesis and assembly of silver nanostructures for plasmonic applications, Chem. Rev. 111 (2011) 3669–3712, https://doi.org/10.1021/cr100275d.
[31] D.P. Birnie 3rd, A model for drying control cosolvent selection for spin-coating uniformity: the thin film limit, Langmuir 29 (2013) 9072–9078, https://doi.org/10.1021/la401106z.
[32] J.M. Luther, M. Law, Q. Song, C.L. Perkins, M.C. Beard, A.J. Nozik, Structural, optical, and electrical properties of self-assembled films of PbSe nanocrystals treated with 1, 2-ethanedithiol, ACS Nano 2 (2008) 271–280.
[33] B.T. Diroll, X. Ma, Y. Wu, C.B. Murray, Anisotropic cracking of nanocrystal superlattices, Nano Lett. 17 (2017) 6501–6506.
[34] L. Wang, Z. Ma, Y. Zhang, L. Chen, D. Cao, J. Gu, Polymer-based EMI shielding composites with 3D conductive networks: a mini-review, SusMat (2021), https://doi.org/10.1002/sus2.21.
[35] V. Shukla, Review of electromagnetic interference shielding materials fabricated by iron ingredients, Nanoscale Adv 1 (2019) 1640–1671, https://doi.org/10.1039/C9NA00108E.
[36] Y. Jiao, S. Cheng, F. Wu, X. Pan, A. Xie, X. Zhu, W. Dong, MOF– guest complex derived Cu/C nanocomposites with multiple heterogeneous interfaces for excellent electromagnetic waves absorption, Compos. B Eng. 211 (2021) 108643, https://doi.org/10.1016/j.compositesb.2021.108643.
[37] H. Li, X. Lu, D. Yuan, J. Sun, F. Erden, F. Wang, C. He, Lightweight flexible carbon nanotube/polyaniline films with outstanding EMI shielding properties, J. Mater. Chem. C 5 (2017) 8694–8698, https://doi.org/10.1039/C7TC02394D.
[38] F. Shahzad, M. Alhabeb, C.B. Hatter, B. Anasori, S.M. Hong, C.M. Koo, Y. Gogotsi, Electromagnetic interference shielding with 2D transition metal carbides (MXenes), Science 353 (2016) 1137–1140. https://www.science.org/lookup/doi/10.1126/science.aag2421.
[39] L. Wu, F. Wu, Q. Sun, J. Shi, A. Xie, X. Zhu, W. Dong, A TTF–TCNQ complex: an organic charge-transfer system with extraordinary electromagnetic response behavior, J. Mater. Chem. C 9 (2021) 3316–3323, https://doi.org/10.1039/D0TC05230B.
[40] L. Wu, A. Xie, F. Wu, J. Shi, Q. Sun, W. Dong, Conductive fibrous metal-cyanoquinone complexes with excellent microwave absorption and shielding effectiveness at ultrathin thickness, Adv. Mater. Interfaces 8 (2021) 2100712, https://doi.org/10.1002/admi.202100712.
[41] N. Li, Y. Huang, F. Du, X. He, X. Lin, H. Gao, Y. Ma, F. Li, Y. Chen, P.C. Eklund, Electromagnetic interference (EMI) shielding of single-walled carbon nanotube epoxy composites, Nano Lett. 6 (2006) 1141–1145, https://doi.org/10.1021/nl0602589.